Nature Communications

https://doi.org/10.1038/s41467-026-68475-4

Article in Press

Structural mechanisms for inhibition and activation of human small-conductance Ca^{2+}-activated potassium channel SK2

Received: 25 July 2025

Accepted: 5 January 2026

Cite this article as: Ma, B., Wu, D., Cao, E. *et al.* Structural mechanisms for inhibition and activation of human small-conductance Ca^{2+}-activated potassium channel SK2. *Nat Commun* (2026). https://doi.org/10.1038/s41467-026-68475-4

Bao Ma, Di Wu, En Cao, Cheng Chi, Zhihao Wang, Zhanyi Xia, Long-Hua Sun, Bingxing Pan, Daohua Jiang & Wenhua Zhang

Structural mechanisms for inhibition and activation of human small-conductance Ca^{2+}-activated potassium channel SK2

Bao Ma[1,2#], Di Wu[2,3#], En Cao[1#], Cheng Chi[4#], Zhihao Wang[1], Zhanyi Xia[2,3], Long-Hua Sun[5], Bingxing Pan[6]*, Daohua Jiang[2,3]*, Wenhua Zhang[1,5,6]*

[1] Jiangxi Institute of Respiratory Disease, The First Affiliated Hospital, and School of Basic Medical Sciences, Jiangxi Medical College, Nanchang University, Nanchang 330031, China

[2] Beijing National Laboratory for Condensed Matter Physics, Institute of Physics, Chinese Academy of Sciences, Beijing 100190, China

[3] University of Chinese Academy of Sciences, Beijing 100190, China

[4] Peking University Institute of Advanced Agricultural Sciences, Shandong Laboratory of Advanced Agricultural Sciences at Weifang, Weifang, Shandong 261000, China

[5] The Department of Respiratory and Critical Care Medicine and Jiangxi Provincial Key Laboratory of Respiratory Diseases, The First Affiliated Hospital, Jiangxi Medical College, Nanchang University, Nanchang, Jiangxi, 330006, P.R. China

[6] Jiangxi Province Key Laboratory of Brain Science and Brain Health, Institute of Biomedical Innovation, Jiangxi Medical College, Nanchang University, Nanchang 330031, China

[#] These authors contributed equally to this work.

* Correspondence: jiangdh@iphy.ac.cn (D.J.); whzhang@ncu.edu.cn (W.Z.); panbingxing@ncu.edu.cn (B.P.)

Abstract

The small-conductance calcium-activated potassium (SK1-3 or $K_{Ca}2$) channels regulate the intrinsic excitability and firing frequency of excitable cells. SK channels are modulated by a variety of distinct modulators; however, the underlying mechanisms remain elusive. Here, we present four cryoelectron microscopy structures of the human SK2-calmodulin complex bound with apamin, UCL1684, AP30663, and CAD-1883, elucidating their distinct binding sites and regulatory mechanisms. Apamin and UCL1684 compete for a similar binding site above the selectivity filter, which is formed by the distinct S3-S4 linker of SK2. CAD-1883 glues the N-lobe of calmodulin and the S4-S5 linker of SK2, reinforcing the open state. In contrast, AP30663 resides in the central cavity of SK2, blocking ion conductance. This study reveals multiple modulation sites in SK2 and the molecular mechanisms for the inhibition and potentiation of SK channels, which could advance rational drug design targeting SK2 channel for the treatment of cardiovascular and neurological disorders.

Introduction

The small-conductance calcium-activated potassium (SK) channels play pivotal roles in regulating cellular excitability and calcium signalling in many tissues by governing the medium afterhyperpolarization (mAHP) phase of action potentials[1-4]. SK channels are involved in numerous physiological activities, including synaptic plasticity, learning and memory, and cardiac pacemaker control[5-7]. The SK channel family comprises three small-conductance channels, SK1 ($K_{Ca}2.1$, encoded by *KCNN1*), SK2 ($K_{Ca}2.2$, encoded by *KCNN2*), and SK3 ($K_{Ca}2.3$, encoded by *KCNN3*) with a single-channel conductance of ~10 pS[8,9], and one intermediate-conductance channel, SK4 (IK1 or $K_{Ca}3.1$, encoded by *KCNN4*) with a single-channel conductance of ~40 pS[10,11]. SK1-3 share a high degree of amino acid identity of over 80%, whereas they are less than 48% identical to SK4. SK1-3 are widely expressed in central and peripheral neurons, but SK4 is largely absent in brain neurons[9,12]. Despite these differences, SK channels are solely activated by submicromolar Ca^{2+} via calmodulin (CaM), which constitutively binds to the intracellular calmodulin-binding domain (CaM-BD) of the channel[13,14]. The structural study of SK4 has revealed the overall homotetrameric architecture and the Ca^{2+}-activation mechanism[15]; that is, the C-lobe of CaM permanently binds to the CaM-BD of SK4, whereas the CaM N-lobe is flexible without Ca^{2+}; after sensing and binding to Ca^{2+}, the N-lobe moves to the S4-S5 linker and pulls the pore-lining S6 to open the gate. Consistent with this mechanism, recent structural studies of rat SK2/CaM[16] and human chimeric SK2-4/CaM[17] revealed similar architecture and assembly to that of the SK4/CaM complex.

The peptide neurotoxin apamin from bee venom is considered the most selective and potent blocker of SK1-3, which has been widely used as an invaluable tool for investigating SK channel properties[6,18-20]. Apamin preferentially blocks SK2 over SK1 and SK3 with at least 10-fold higher affinity and, remarkably, is ineffective on SK4[8,10,11,21,22]. Mutagenesis studies suggest that apamin sensitivity is largely determined by several residues in the outer vestibule[23-26]. Moreover, *d*-tubocurarine, dequalinium and its bis-quinolinium cyclophane derivatives UCL1684 and UCL1848

also block SK1-3 via occupation of the apamin site[23,27-30]. However, the precise binding site of apamin in SK channels and its mechanism of action remain undefined.

Because of their physiological importance, SK1-3 have been implicated as attractive therapeutic targets for the treatment of atrial fibrillation, ataxia, epilepsy, anxiety disorders, and neurodegenerative diseases[1,3,4,31,32]. Many small-molecule modulators that alter SK channel functions are emerging[32], several of which have advanced to clinical trials to explore their therapeutic potential. For instance, AP30663, a novel nonselective SK1-3 negative modulator[33], has recently completed Phase I and Phase II clinical trials to evaluate its efficacy in treating atrial fibrillation[34-36], demonstrating positive results. Moreover, CAD-1883 (also known as rimtuzalcap), a positive modulator of SK channels, has undergone two Phase II clinical trials to investigate its potential to alleviate movement disorders, including spinocerebellar ataxia (Phase II: NCT04301284) and essential tremor (Phase II: NCT03688685). These clinical investigations highlight the growing interest in SK channels as therapeutic targets. Previous structural analysis suggested that SK channel activators such as NS309 and riluzole bind to the interface of CaM and the isolated CaM-BD of SK2[37-39]; however, this model contradicts the binding mode of CaM revealed by the full-length SK4/CaM structure[15]. Therefore, the mechanisms of action for the inhibition and potentiation of SK channels by these clinical compounds are unknown, and the lack of the desired SK-drug complex structure hampers further optimization of these compounds to achieve better efficacy.

In this work, we have solved four cryoelectron microscopy (cryo-EM) structures of the human SK2-calmodulin complex bound with apamin, UCL1684, CAD-1883, and AP30663, respectively, revealing three distinct modulation sites in SK2 and their detailed modes of action. Augmented with mutagenesis studies and electrophysiological functional analysis, this work revealed that apamin sensitivity is endowed by the distinct S3-S4 linker of SK2 and provides the structural basis for the activation, inhibition, potentiation, and pharmacology of SK channels, which opens new avenues for precise therapeutic development to treat a variety of SK channel-related diseases.

Results

Structures of SK2–CaM bound with modulators

To explore the structural pharmacology of SK2, we purified human wild-type (WT) full-length SK2 coexpressed with human CaM in HEK293F cells and analyzed the detergent-purified samples by cryo-EM. However, the human WT SK2 exhibited structural heterogeneity in the intracellular domain, which hindered high-resolution structure determination. After optimization, we found that the addition of 2 mM Ca^{2+} and excess purified CaM substantially improved the sample quality of human SK2/CaM, as reflected by the association of CaM with SK2 through purification (Supplementary Fig. 1a,b). We next performed cryo-EM single-particle analysis of the purified samples in the presence of apamin, UCL1684, CAD-1883 or AP30663 and determined the SK2-CaM structures in complex with CAD-1883 (SK2-CAD-1883), apamin (SK2-apamin), UCL1684 (SK2-UCL1684), and AP30663 (SK2-AP30663) at resolutions of 3.35 Å, 3.23 Å, 2.96 Å, and 3.34 Å, respectively (Supplementary Figs. 1-4). The density maps permit reliable model building of the SK2 TM core region for all four structures and the placement of the respective modulators; however, CaM can be assigned only to the activator-bound SK2-CAD-1883, whereas the C-lobe of CaM is partly flexible, and the N-lobe is completely invisible in the other three structures (Fig. 1a,b and Supplementary Fig. 5), indicating that SK2-CAD-1883 adopts an open conformation, whereas SK2-apamin, SK2-UCL1684, and SK2-AP30663 are in a closed state. Because the CAD-1883-bound structure contains a more complete model for both SK2 and CaM than the other three structures do, it was selected for subsequent structural description and comparison.

The overall structure of SK2-CaM resembles the SK4-CaM structure (PDB ID: 6CNN)[15] with a root mean square deviation (r.m.s.d.) of 2.6 Å between 1833 aligned Cα atoms. The homotetrameric SK2 is organized in a domain nonswapped manner, and each protomer comprises a voltage sensor-like domain (S1-S4) and a pore domain (S5-S6), which are connected by the S4-S5 linker consisting of two short α helices (S_{45}A and S_{45}B). The pore lining S6 is

extended into two long chopstick-like HA and HB helices that are parallel to the membrane plane. Notably, the hairpin-like S3-S4 linker is clearly resolved and points to the central axis, four of which together constitute the outer vestibule of SK2 (Fig. 1b,c and Supplementary Figs. 2f,3d). The C-lobe of CaM holds onto the HA helix of one protomer, whereas the N-lobe engages with the $S_{45}A$ helix of the opposing protomer (Fig. 1b,c), which is consistent with the observations in the Ca^{2+}-bound SK4–CaM structure[15].

The superposition of the SK2 and SK4 structures revealed that the TM core regions closely resemble each other, but the loop regions exhibited marked structural differences. In particular, the S3-S4 linker of SK2 forms a pair of antiparallelly arranged β sheets; in contrast, the S3-S4 linker of SK4 is unstructured and invisible to cryo-EM (Fig. 1d). The outer vestibule formed by these linkers in SK2 plays a vital role in apamin binding, as shown below. Additionally, S5 and S6 of SK2 are covalently linked by a disulfide bond between C332 and C370, which is absent in SK4 (Fig. 1d). Furthermore, an extra density in the space between S4 and S6 of SK2 suggests the binding of a possible cholesterol molecule (Fig. 1d), where a detergent-like molecule binds to SK4[15]. Interestingly, the density maps at the equivalent position of the three inhibitor-bound closed SK2 structures fit a possible phospholipid, likely because of local conformational shifts between the open and closed SK2 structures (Supplementary Fig. 4h-i).

Structural basis for SK2 blockade by apamin and UCL1684

Apamin is an 18-residue peptide neurotoxin that can potently and selectively inhibit SK2[8,21]. Structural analysis revealed that apamin consists of an N-terminal loop and a C-terminal helix[40-42], which are linked by two cysteine disulfide bonds, Cys_1-Cys_{11} and Cys_3-Cys_{15} (Fig. 2a). Our whole-cell patch-clamp recording results revealed that apamin gradually reduced SK2 currents, resulting in an IC_{50} of 120.6 ± 29.2 pM (Fig. 2b), which is comparable to the results of previous studies[8,21,22,26].

A large piece of strong density was observed in the outer vestibule of SK2-apamin but not in SK2-CAD-1883 or SK2-AP30663, which fits the entire C-terminal helix and partly covers the N-

terminal loop of apamin, demonstrating the binding of one apamin to the tetrameric SK2 (Figs. 1a, 2c and Supplementary Fig. 5a,5f). Because of this configuration, we only imposed C1 symmetry during density map refinements. However, the poor density of the N-loop is more likely due to its intrinsic flexibility, not the use of C1 symmetry (Supplementary Figs. 1e and 5a). The outer vestibule of SK2 has a negatively charged surface potential that matches the positive side of apamin, reinforcing their strong interactions (Supplementary Fig. 5c). The SK2-apamin structure clearly elucidates that apamin binding completely blocks the ion pathway from the extracellular side.

Apamin is tightly embraced by the four S3-S4 linkers, which are flexible in SK4, explaining why SK4 is insensitive to apamin (Figs. 1d,2d). The long antiparallel S3-S4 linkers are stabilized by extensive interactions. Specifically, R240 participates in electrostatic interactions with the backbone carbonyl oxygens of Q339 and D340 from the neighboring protomer; Y245 interacts with the backbone carbonyl of A242 (Fig. 2e). In addition, H336 of the pore loop forms a hydrogen bond interaction with S248, and van der Waals contracts with W237; N367 of the pore loop engages in polar interactions with the backbone nitrogen of A242 (Fig. 2e). We speculate that these specific interactions stabilize the conformation of the S3-S4 linker, providing a proper chemical and geometric environment for the binding of apamin. Consistent with this hypothesis, although H336 and N367 have no direct contact with the bound apamin in the SK2-apamin structure, previous studies have showed that mutating H337 at the equivalent position in rat SK2 with Asn or Arg greatly impaired apamin potency[23,25]. The nonconserved N367 is substituted by His in SK1 and SK3 (Supplementary Fig. 6a). We showed that 300 nM apamin inhibited the H336N and N367H mutants by only ~20% and ~60%, respectively (Fig. 2g,h and Supplementary Fig. 7h). We further generated the R240A, A242F, and Y245A mutations and investigated the inhibitory effects of apamin on these functional mutants (Supplementary Fig. 7h). Although these residues are not involved in apamin binding, A242F is insensitive to 300 nM apamin, and the apamin dose–response curves revealed IC_{50} values of 11.8 ± 4.5 nM in R240A and 3.7 ± 1.2 nM in Y245A, which are approximately 98- and 31-fold less potent than that in WT SK2, respectively

(Fig. 2g,h). The AlphaFold2[43] models suggest that the S3-S4 linkers of SK1-3 adopt a similar fold to that of our SK2 structure. We speculate that several nonconserved residues, including S244 in the S3-S4 linker and N367 in the pore loop, could affect the conformation of the S3-S4 linker, which is crucial for apamin binding, resulting in the apamin sensitivity gap in SK1-3.

A closer look at the apamin binding site revealed that Arg_{13} and Arg_{14} of apamin stick their long side chains into the space between two adjacent F243 of the S3-S4 linkers, forming cation–π interactions with F243 and electrostatic interactions with the backbone carbonyl oxygens of G362 and D363 from the selectivity filter; meanwhile, Leu_{10}, Gln_{17} and His_{18} interact with the channel and contribute to apamin binding (Fig. 2d). This observation coincides well with the fact that Arg_{13} and Arg_{14} are critical for apamin binding and toxic activity[44]. In addition, apamin also makes close contacts with S244 of the S3-S4 linker (Fig. 2e). To validate these structural findings, we generated the S244F and F243A mutants and assayed their response to apamin. Both the S244F and F243A mutants elicited currents comparable to that of WT SK2; however, the F243A was almost completely insensitive to 300 nM apamin, and the S244F was inhibited only approximately 40% by 300 nM apamin (Fig. 2g,h and Supplementary Fig. 7h). Of note, S244 is not conserved in SK1-3 and is replaced by T216 in human SK1. Previous studies demonstrated that mutating S245 at the equivalent position in rat SK2 with a Thr impaired apamin potency by ~7.5-fold and that the T216S mutation in human SK1 increased the apamin sensitivity of human SK1[24,26], indicating that S244 is one of the determinants contributing to the differences in the potency of apamin in SK1-3.

Organic compounds such as *d*-tubocurarine and dequalinium have been shown to competitively displace apamin binding[23,27,32]. We assayed the dose-dependent inhibition of SK2 by the high-affinity bis-quinolinium cyclophane derivative UCL1684, which yielded an IC_{50} of 3.1 ± 1.1 nM (Supplementary Fig. 7a,b), in line with the findings of a previous study[29]. To elucidate the relationship between apamin and UCL1684 binding in SK2, we determined the SK2-CaM structure in complex with UCL1684 (Supplementary Figs. 2 and 7c). Similar to SK2-apamin, strong nonproteinaceous density appears in the outer vestibule of SK2-UCL1684, which could

accommodate one UCL1684 molecule (Supplementary Fig. 7c,d). UCL1684 is situated in the outer vestibule, where it forms extensive contacts, mainly with the four F243 residues (Fig. 2f). The binding of UCL1684 fully occludes the ion path, reminiscent of the action of apamin (Fig. 2d,f). The superposition of SK2-apamin and SK2-UCL1684 revealed that UCL1684 binds deeper in SK2 than does apamin, and interestingly, the two positive quinolinium rings are positioned similarly to Arg_{13} and Arg_{14} of apamin (Supplementary Fig. 7e-f). This observation implies that the two shared positive rings in *d*-tubocurarine, dequalinium and the bis-quinolinium cyclophane derivatives play critical roles in inhibiting SK channels. Our mutagenesis results revealed that F243A and H336N greatly impaired the efficacy of 1 μM UCL1684, similar to their response to 300 nM apamin; however, the A242F, S244F, Y245A and N367H mutants could still be largely inhibited by 1 μM UCL1684, whereas their sensitivity to 300 nM apamin substantially decreased (Fig. 2g and Supplementary Fig. 7i). These results are in accordance with the structural observation that the peptide apamin participates in broader interactions with the S3-S4 linker than does UCL1684 (Fig. 2d,f).

Two recent studies revealed that apamin and UCL1684 bind to the extracellular vestibule of rat SK2 and human chimeric SK2-4 channels[16,17]. Importantly, structural comparisons demonstrated very similar binding modes for apamin and UCL1684 in these SK2 structures, although the intracellular gate and selectivity filter of these structures assume different conformations (Supplementary Fig. 8a-f), suggesting that apamin and UCL1684 are state-independent blockers.

Structural basis for SK2 potentiation by CAD-1883

CAD-1883 (also called rimtuzalcap), a positive allosteric modulator of SK channels, has undergone two Phase II clinical studies for the treatment of essential tremors and spinocerebellar ataxia (Fig. 3a). To reveal the mechanism of action of CAD-1883, we first investigated the concentration-dependent potentiation of SK2 by CAD-1883 via whole-cell patch clamp recording of SK2-expressing HEK293T cells. When the internal Ca^{2+} concentration was ~300 nM, the

currents of SK2 were gradually increased by CAD-1883, yielding an EC_{50} value of 2.7 ± 1.3 μM (Fig. 3b). We next determined the cryo-EM structure of SK2-CaM bound to CAD-1883 at a resolution of 3.35 Å with C4 symmetry (Supplementary Fig. 3). In contrast to the closed SK2-apamin and SK2-UCL1684, the density maps for the four complete CaM molecules are clearly resolved in SK2-CAD-1883, indicating a different state (Fig. 1a and Supplementary Fig. 5). Most importantly, the strong nonproteinaceous density in each of the CaM N-lobes unambiguously elucidated the binding of CAD-1883 (Fig. 3c and Supplementary Fig. 3d).

In the SK2-CAD-1883 complex structure, CAD-1883 resides in a pocket formed by the CaM N-lobe, S4-S5 liker helix, and HA helix from the adjacent subunit and places its difluorocyclohexane and pyrimidine moieties on the CaM N-lobe, the methylpyrazole group pointing towards SK2, and the morpholine group facing intracellular solvents (Fig. 3c,d). More specifically, the difluorocyclohexyle and pyrimidine moieties engage in extensive hydrophobic interactions with L291 from SK2 and F19, L32, M36, M51, F68, and M71 from the N-lobe of CaM; the methylpyrazole group interacts with I288, N292, and F409 from SK2 as well as L39 and Q41 from CaM (Fig. 3c,d). Sequence alignment revealed that these residues responsible for CAD-1883 binding are highly conserved among SK1-4, suggesting that CAD-1883 may be a nonspecific potentiator for SK channels (Supplementary Fig. 6). To validate this CAD-1883 binding site, we generated the L291F, L291W, and L291A/N292A mutations and assayed their currents elicited by 1 μM internal Ca^{2+}. Although the activation kinetics of these mutants remain similar to that of WT SK2, all the mutants display reduced currents compared with WT SK2 (Supplementary Fig. 9a). However, none of them can be strongly activated by 100 μM CAD-1883 (Fig. 3e-h and Supplementary Fig. 9b), suggesting that introducing steric hinderance by L291F or L291W and abolishing the polar interaction from N292 may impair the binding of CAD-1883 in the pocket.

Our pore radius analysis clearly revealed that SK2-apamin is closed and that SK2-CAD-1883 has an intracellular gate with a van der Waals diameter of ~8 Å (Fig. 3i,j), indicating that SK2-CAD-1883 was captured in an open state. In particular, the intracellular gate of SK2-apamin is

sealed by four V390 residues from the S6 helices, which undergo a conformational shift and rotation in SK2-CAD-1883, resulting in a dilated open gate (Supplementary Fig. 9c-e). Moreover, the gate of SK2-CAD-1883 resembles the open gates of rat SK2 and SK4 activated-II[15], and is notably wider than those of the closed SK4 and the activated-I SK4 (Supplementary Figs. 8k and 9f-h). Structural comparisons revealed that the CAD-1883-bound SK2 closely resembles the fully opened rat SK2 and SK4 activated-II structures and exhibits marked conformational differences in the S4-S5 linker, S6, and the N-lobe of CaM compared with the closed SK2-apamin, closed SK4, and SK4 activated-I (Fig. 3k and Supplementary Figs. 8j-l and 9i-k). Although both are in the open state, CAD-1883 binding still induces outward conformational shifts of the CaM N-lobe relative to the open SK4, facilitating closer interactions between the S_{45}A helix of SK2 and the CaM N-lobe (Fig. 3k).

These structural observations elucidate that CAD-1883 functions as a glue-like molecule that promotes the recruitment of the CaM N-lobe to the S_{45}A helix, thereby stabilizing the SK2 channel in this specific open state.

Structural basis for SK2 inhibition by AP30663

AP30663 is a potential antiarrhythmic agent that has been investigated in Phase II clinical trials for the treatment of atrial fibrillation. To understand how AP30663 inhibits SK2 channel, we first tested the concentration-dependent inhibition of SK2 by AP30663, which resulted in an IC_{50} value of 0.99 ± 0.14 μM, in line with a previous study[33] (Fig. 4a,b). We next purified SK2-CaM samples in the presence of AP30663 and solved the cryo-EM structure at 3.34 Å resolution with C1 symmetry imposed (Supplementary Fig. 4). The EM density map allows the model building of SK2, but the density for the CaM is weak, similar to that in SK2-apamin and SK2-UCL1684 (Fig. 4c and Supplementary Fig. 5). We observed strong extra density in the central cavity of SK2-AP30663, which can accommodate an AP30663 molecule and is not present in the central cavity of SK2-apamin or SK2-UCL1684 (Fig. 4d). The density map is not sufficient for unambiguous placement of AP30663, presumably because of the binding of an asymmetric blocker on the

fourfold symmetric axis of the channel, a similar situation that has also been reported in a recent AP14145-bound rat SK2 study[16] and other fourfold symmetric channels[45]. The SK2-AP30663 structure strongly indicates that AP30663 binds to the central cavity beneath the selectivity filter and serves as a pore blocker (Fig. 4c,e).

AP30663 resides in the central cavity with an orientation nearly perpendicular to the membrane plane and is sandwiched by four S358 residues from the top and four A383 and four T386 residues from the bottom (Fig. 4e). In this potential binding pose, the cyano group of AP30663 forms a possible polar interaction with the backbone carbonyl oxygen of G379, and the compound's core region engages in van der Waals interactions with S358, A383, and T386 (Fig. 4e). S358 and A383 are not conserved in SK4, which are substituted by T250 and V275, respectively, which potentially explains the finding that the S508T/A532V double-site mutation in rat SK3 (corresponding to S358 and A383 in SK2) reduces AP14145 (a close analog of AP30663) inhibition by ~70%, and the T250S/V275A mutation confers AP14145 sensitivity to the insensitive human SK4 channel[46] (Supplementary Fig. 6a). To further probe the functional role of A383 and to the best of our knowledge the previously uncharacterized T386, we assayed the inhibitory effects of AP30663 on the A383F, A383L, T386L, T386F and T386A mutants and found that 30 μM AP30663 strongly inhibited the A383L mutant, similar to WT SK2, whereas it inhibited the A383F, T386L, and T386F mutants by only ~25%, ~15%, and ~40%, respectively (Fig. 4f and Supplementary Fig. 10a-e). T386A, however, greatly reduced the peak current of SK2 to less than 0.5 nA, which prevented further investigation of its effect on AP30663 (Supplementary Fig. 10f). We next determined the concentration–response inhibition curve for A383L, which yielded an IC_{50} value of 2.1 ± 0.6 μM, suggesting a moderate reduction in the potency of AP30663 in the inhibition of A383L compared with WT SK2 (Fig. 4g,h). Collectively, these functional results demonstrate that AP30663 exerts its inhibitory effect on SK1-3 channels by directly blocking the central cavity and that three key residues (S358, A383, and T386) play critical roles in AP30663 binding and specificity against SK4.

Ca^{2+}-activation and modulation mechanisms of SK2

The SK2 cryo-EM structures of this study and two recent SK2 studies[16,17] revealed a conserved Ca^{2+}-dependent gating mechanism in SK channels, which is consistent with the SK4 channel[15]. In the resting state, the C-lobe of CaM constitutively binds to the HA helix of the CaM-BD, whereas the N-lobe of CaM is mobile; thus, the intracellular gate of SK assumes a closed conformation (Fig. 5a). When intracellular Ca^{2+} surges to submicromolar concentrations, Ca^{2+} ions bind to the N-lobe of CaM and induce conformational changes in CaM, resulting in engagement between the N-lobe and the $S_{45}A$ helix of the adjacent SK2 subunit and pulling the $S_{45}A$ helix downwards by ~3 Å (measured at the Cα atom of N292). This displacement forces the $S_{45}B$ and S6 helices to move away from the pore axis, thereby dilating the cytoplasmic activation gate from a radius of 5.3 Å to 10.7 Å, which allows the permeation of hydrated K^+ ions (Fig. 5b and Supplementary Fig. 9c-e).

Our modulator-bound SK2 complex structures reveal three distinct modulation sites in SK2 (namely, Sites 1-3). At Site 1, apamin and UCL-1684 can bind to the extracellular vestibule formed by the distinct S3-S4 loop of SK2 channel, which physically blocks the exit of K^+ ions (Fig. 5c). The central site is referred to as Site 2, in which AP30663 and its analogs reside, preventing K^+ access to the selectivity filter (Fig. 5c). Unlike physical blockade by inhibitors bound to Sites 1 and 2, Site 3 harbors positive allosteric modulators such as CAD-1883 and NS309, which facilitate the opening of SK2 and stabilize the open state (Fig. 5c).

In the closed structure of SK2-apamin, strong EM densities indicate that four putative K^+ ions are coordinated by the backbone carbonyl oxygen atoms of the conserved “XXGYG” motif in the selectivity filter (Supplementary Fig. 11a,b). In contrast, the activated SK2-CAD-1883 structure possesses a disrupted selectivity filter, of which Y361 underwent a 180° rotation, resulting in dramatic dilation at the positions of G360 and Y361 and discontinued K^+ sites in the selectivity filter (Supplementary Fig. 11c-e). The dilated selectivity filter of SK2-CAD-1883 is reminiscent of the structure of the Shaker K_V channel with a W434F mutation[47], which is proposed in a C-type inactivated state (Supplementary Fig. 11f-h). Moreover, the dilated selectivity filter with a rotation of the conserved Tyr has also been observed in the UCL1684-bound rat SK2 structure with an

open intracellular gate and the chimeric human SK2-4 structures with (open) or without (closed) calcium ions[16,17] (Supplementary Fig. 8d-l). We speculate that the SK2-CAD-1883 structure may represent an inactivated state because the binding of CAD-1883 consistently activates the intracellular gate that may eventually inactivate the channel by altering the conformation of the selectivity filter.

Discussion

In this study, we presented four cryo-EM structures of human WT SK2-CaM in complex with apamin, UCL1684, and two clinically investigated modulators, AP30663 and CAD-1883. We found that the human WT SK2 channel is rather difficult for structural studies. A major problem is that CaM is not consistent bound to SK2 after detergent purification, regardless of the presence or absence of Ca^{2+}. This incomplete binding of CaM caused structural heterogeneity in the intracellular domains of the complex, which prevented us from obtaining high-resolution SK2 structures. A similar problem in human WT SK2 channel was reported by Cassell *et al.*[17]. After optimization, we found that the addition of excess purified CaM to the purified SK2 samples increased the amount of CaM associated with SK2, which eventually led us to solve the modulator-bound SK2 structures. Alternatively, Nam *et al.* used rat SK2, and Cassell *et al.* constructed a human SK2 chimera by replacing the N-terminus and the C-terminal CaM binding helices with those of SK4 for structural analysis[16,17]. Of note, even in the presence of 2 mM Ca^{2+}, our three inhibitor-bound SK2 structures were captured in the closed state, whereas the CAD-1883-bound structure adopted the open conformation, suggesting that CAD-1883 reduced the energy barrier of Ca^{2+}-dependent activation of the human SK2 channel in solution.

Although the binding mode of CaM and the Ca^{2+}-dependent activation mechanism of SK2 are in accordance with those of the SK4 channel[15], SK2 channel exhibits marked structural differences compared with SK4. First, the CaM-BD and the associated CaM in SK2 appear to be more dynamic than those in SK4 in the closed state, as reflected by the invisible density for the CaM N-lobe and the weak density for the HA and HB helices (Supplementary Fig. 5). Second, the four S3-S4 linkers of SK2 form an extra extracellular vestibule above the selectivity filter, whereas the S3-S4 linker in SK4 is flexible. This outer vestibule not only determines the binding of apamin and UCL-1684 but also has a role in controlling the conductance of SK2. In a recent related study, mutating F244 of rat SK2 (equivalent to F243 in human SK2) to serine increased the unitary conductance to a level similar to that of the intermediate-conductance SK4 channel[16].

Our SK2-apamin structure defines the long-awaited binding pocket for the SK2-specific toxin apamin, revealing the detailed interactions between apamin and SK2 and its mechanism of action. Apamin fully occupies the extracellular vestibule and completely blocks the exit of K^+ (Fig. 2d), suggesting that apamin is not an allosteric modulator. Several variable residues among SK1-3, including S244 and N367, directly affect apamin binding or indirectly alter the conformation of the outer vestibule, most likely determining the SK2-specific property of apamin[24-26]. Additionally, UCL-1684 also binds to the extracellular vestibule, a binding mode that largely overlays apamin, explaining the competitive relationship of UCL-1684 and apamin in inhibiting SK2 channel[23,27]. Because UCL-1684 is smaller than apamin, it can bind deeper in the pocket than apamin does (Supplementary Fig. 7e). Although the SK2 samples were prepared differently, structural comparisons elucidated consistent binding modes for apamin and UCL1684 in these structures (Supplementary Fig. 8). We further demonstrated that AP30663 functions as a pore blocker that binds to the central cavity of SK2, which is consistent with the findings of a recent study suggesting that AP14145, a close analog of AP30663, binds to the central cavity of the rat SK2 channel[16]. The SK2-AP30663 structure indicates that the central cavity of SK2 prefers flat molecules and that S358 and A383 dictate the subtype selectivity of AP30663 for the SK1-3 channels over the SK4 channel[46]. Moreover, the SK2-CAD-1883 structure demonstrated that CAD-1883 acts as a molecular glue that strengthens the engagement of the CaM N-lobe with the S_{45}A helix of SK2, thereby promoting the opening of the intracellular activation gate. However, the residues involved in CAD-1883 binding are highly conserved in SK1-3 channels, suggesting that CAD-1883 is a nonselective potentiator of SK1-3 channels. These SK2 structures could serve as templates for optimizing CAD-1883 and AP30663 to achieve better affinity and efficacy.

In summary, these structures provide important mechanistic insights into Ca^{2+}-dependent activation, inhibition and potentiation of SK2 channel, which not only expand the understanding of the structural pharmacology of SK channels but also provide a solid foundation for the rational development of therapeutics targeting SK channels for the treatment of neurological and cardiovascular disorders.

Methods

Construct design

The cDNA fragments encoding human SK2 (*KCNN2*; UniProt ID: Q9H2S1) and calmodulin (*CALM1*; UniProt ID: P0DP23) were synthesized and inserted into the pBIG1a vector using biGBac method with a C-terminal tag containing an HRV3C protease cleavage site, an mCherry fluorescence protein and a Twin-Strep II affinity tag. This multigene construct of the SK2/CaM complex was used for protein-expression. To monitor and increase the expression of CaM, the CaM gene was cloned into a modified pEG BacMam vector followed by an internal ribosome entry site (IRES) and a superfolder green fluorescent protein at C-terminus. For the expression and purification of human CaM alone, the cDNA fragment encoding calmodulin was inserted into a pET28a vector, featuring an N-terminal 8×His tag and an HRV 3C protease cleavage site. For electrophysiological recording, the cDNA fragments encoding SK2 was cloned into modified pEG BacMam vector, followed by an IRES and a mCherry fluorescent protein. Point mutations were generated by a standard site-directed mutagenesis kit (Vazyme Biotech Co., Ltd.). All the constructs were confirmed by DNA sequencing.

Protein expression and purification

For CaM purification, CaM-expressing *E. coli* cells were resuspended in buffer containing 50 mM Tris (pH 8.0), 150 mM NaCl, 0.1% v/v Triton X-100, 10% v/v glycerol, 10 mM imidazole, 10 mM β-mercaptoethanol, 1 mM PMSF, 0.05 mg/ml DNase I and homogenized via a high-pressure homogenization three times. The lysate was centrifuged at 100,000 × g for 1 h. The supernatant was filtered through a 0.22 μm membrane and subsequently loaded onto Ni-NTA 6FF Beads (Smart-Lifesciences, China) at 4°C. The resin was washed with 10 column volumes of first wash buffer (50 mM Tris pH 8.0, 500 mM NaCl, 10% v/v glycerol, 10 mM imidazole, 10 mM β-mercaptoethanol, 1 mM PMSF) and second wash buffer (50 mM Tris pH 8.0, 150 mM NaCl, 10% v/v glycerol, 30 mM imidazole, 10 mM β-mercaptoethanol, 1 mM PMSF). CaM proteins were eluted with the second wash buffer supplemented with 250 mM imidazole. The 8×His tag was cleaved by 3C protease at a ratio of 1:20 (w/w). The solution was reapplied to Ni-NTA 6FF beads

to remove the cleaved His-tag and protease. To eliminate imidazole, the proteins were dialyzed in buffer containing 50 mM Tris pH 8.0, 150 mM NaCl, 20% v/v glycerol, 1 mM DTT and concentrated using a 10 kDa Amicon Ultra centrifugal filter (Merck Millipore, Germany). The final CaM samples were concentrated to ~5 mg/mL and stored at −80 °C.

For protein expression, recombinant baculoviruses were generated in *Sf9* (Invitrogen, USA) cells using the Bac-to-Bac baculovirus expression system (Invitrogen, 11496015). Subsequently, 1%(v/v) SK2 and 1%(v/v) CaM P3 recombinant baculovirus were cotransfected into HEK293F (FreeStyle 293F cells, Gibco, USA) cells at a density of 2.5×10^6 per mL, supplemented with 1% (v/v) fetal bovine serum. After culture at 37 °C with 5% CO_2 for 12 h, the mammalian cells were supplied with 10 mM sodium butyrate and were further incubated for another 60 h at 30°C. The cells were then harvested by centrifugation at 1640 × g for 5 min, and finally stored at −80°C after being flash-frozen in liquid nitrogen.

For all the purification processes, cells pellets expressing SK2 and CaM complexes were resuspended and homogenized in buffer A (20 mM HEPES pH 7.5, 150 mM KCl, 2 mM $CaCl_2$, 2 mM β-mercaptoethanol (β-ME), 1 mM PMSF, 0.05 mg/mL DNase, aprotinin (2 μg/mL), leupeptin (1.4 μg/mL), pepstatin A (0.5 μg/mL)). The cell membrane was collected by ultracentrifugation at 100,000 × g for 1 h. Subsequently, the membrane pellets were homogenized and solubilized with buffer B (buffer A supplemented with 1% (w/v) n-Dodecyl-β-D-Maltopyranoside (DDM, Anatrace), 0.15% (w/v) cholesteryl hemisuccinate (CHS, Anatrace), 5 mM $MgCl_2$ and 2 mM ATP) for 2 h at 4 °C. The insoluble material was removed by ultracentrifugation at 100,000 × g for 30 min and the supernatant was filtered through 0.22 μm filters to remove cell debris. The supernatant was then loaded onto Streptactin Beads (Smart-Lifesciences, China) via gravity flow at 4°C to enrich the protein complex. The resin was subsequently washed with 10 column volumes of buffer C (buffer A supplemented with 0.01% (w/v) Lauryl Maltose Neopentyl Glycol (LMNG, Anatrace), 5 mM $MgCl_2$ and 2 mM ATP) and another 10 column volumes of buffer D (buffer A supplemented with 0.01% (w/v) LMNG). The protein was eluted with buffer E (buffer D supplemented with 10 mM desthiobiotin (Sigma, USA)). The mCherry and twin-strep tag was cleaved by PreScission

protease at a ratio of 1:20 (w/w). Purified calmodulin was added to the purified SK2 samples to enhance complex formation at a final molar ratio of 1:4 (monomer/monomer). The mixture was incubated on ice for 2 h and then concentrated to 1 mL using a 100 kDa cut-off Amicon ultracentrifugal filter (Merck Millipore, Germany) and subjected to a size-exclusion chromatography column (Superose 6 Increase 10/300 GL (Cytiva)) preequilibrated with the buffer E (20 mM HEPES pH 7.5, 150 mM KCl, 2 mM β-ME, 2 mM $CaCl_2$, 0.005%(w/v) LMNG). The peak fractions were pooled and concentrated to ~2.5 mg/mL for cryo-EM sample preparation. To purify ligand-bound complexes, different ligands including Apamin (MedChemExpress), UCL1684 (Merck), CAD-1883 (MedChemExpress) and AP30663 (MedChemExpress), were mixed with the SK2-CaM sample for at least 30 min, respectively. The final concentrations of apamin, UCL1684, CAD-1883 and AP30663 were controlled to 100 μM, 500 μM, 500 μM, and 500 μM, respectively.

Cryo-EM sample preparation and data acquisition

Aliquots of 4 μL purified ligand-bound SK2 complex samples were applied to holey grids (Cu R1.2/1.3, 300 mesh, Quantifoil) glow discharged by PELCO easiGlow (Ted Pella). The grids were blotted for 3.5-5.0 s at 4°C with 100% humidity using an FEI Vitrobot Mark VI (Thermo Fisher Scientific) and were plunge-frozen in liquid ethane cooled with liquid nitrogen.

Cryo-EM data were collected using a Titan Krios G4 electron microscope operated at 300 kV (Thermo Fisher Scientific) equipped with a K3 direct electron detector (Gatan) and a Quantum GIF energy filter with a slit width of 10 e^-V. All movie stacks were automatically acquired using EPU at a calibrated magnification of 105,000× under superresolution mode with a physical pixel size of 0.85 Å pix^{-1}. Each movie was fractionated into 40 frames with an exposure time of 2.89 s. The defocus range was set between -1.0 and -2.0 μm. In total, 1,268, 5,043, 3,837, and 2,944 cryo-EM movie stacks were collected for SK2-apamin, SK2-UCL1684, SK2-CAD-1883, and SK2-AP30663, respectively.

Cryo-EM data processing

All the data were processed via CryoSPARC[48]. The raw movie stacks were motion-corrected, dose-weighted and binned by 2-fold using Patch Motion correction, followed by a contrast transfer function (CTF) estimation using Patch CTF. Micrographs with a resolution better than 4 Å and astigmatism lower than 500 Å were selected for further data processing. Particles were picked based on 2D templates generated by the SK4/CaM map. Subsequently, particle extraction was carried out with a box size of 320 pixels and a binning factor of 2. The particles were subjected to several rounds of 2D classification to remove ice and junk particles. A set of 2D averages with clear transmembrane features was subjected to ab-initio reconstruction with 3 classes. The optimal map served as the initial reference for performing heterogeneous refinement with C1 symmetry, using all picked 2-fold binned particles as input. Particles from 2D classification with clearly resolved transmembrane helices were selected, re-extracted with a box size of 320 pixels, followed by a non-uniform refinement and rounds of resolution gradient heterogeneous refinement with C1 symmetry. Finally, a round of 3D classification with a promoter mask or transmembrane mask was employed to improve the ligand density, resulting in 3D reconstruction maps at resolutions of 3.23 Å with C1 symmetry, 2.96 Å with C2 symmetry, 3.35 Å with C4 symmetry, 3.34 Å with C1 symmetry for SK2-apamin, SK2-UCL1684, SK2-CAD-1883, and SK2-AP30663, respectively. Similar procedures were used for all data processing, as summarized in Supplementary Figs. 1-4.

Model building and refinement

The AlphaFold2 model of human SK2 and the structure of human CaM (PDB code: 6CNN) served as initial models and were placed into the EM density map of SK2-apamin by rigid-fitting in UCSF Chimera[49], followed by manual correction in Coot[50], which was used as a reference for model building of all four SK2 structures. The refinements of the SK2 models against the EM density maps were further refined in real space using phenix[51]. The models and geometric constraints for UCL1684, AP30663 and CAD-1883 were generated using eLBOW module in Phenix. The apamin structure (PDB code: 7OXF) was used as an initial model. Apamin, UCL1684,

AP30663 and CAD-1883 were manually fitted into their respective density maps. All modulator-bound SK2 structures were refined and validated in Phenix with reasonable geometry restraint parameters and clash scores. The FSC curves of the model versus the map were calculated by Phenix.mtrage. The cryo-EM data collection, refinement and validation statistics are presented in Supplementary Table 1. All figures were prepared with Prism (GraphPad software), ChimeraX[52] and PyMol (Schrödinger, LLC).

Patch clamp electrophysiology

Whole-cell patch-clamp recordings were performed on HEK293T (Gibco, USA) cells transiently transfected with plasmids of WT SK2 or its variants. Currents were recorded using an EPC-10 amplifier (HEKA, Lambrecht, Germany) and acquired via Pulse/Pulsefit software (HEKA, Lambrecht, Germany). All the recordings were conducted at room temperature. Patch pipettes were pulled from borosilicate glass using a horizontal electrode puller (Model P-1000, Sutter Instruments, USA), with a resistance of 3-6 MΩ when filled with intracellular solution (compositions described below). The same bath (external) solution was used for all the current recording experiments in this study, which contained (in mM): 120 KCl, 10 HEPES, 10 EGTA, 6.19 $CaCl_2$ (estimated free [Ca^{2+}], 60 nM), 1.44 $MgCl_2$, pH 7.4, adjusted with KOH. For functional validation of SK2 variants and testing the inhibitory effects of apamin, UCL1684 and AP30663, the pipette (internal) solution contained (in mM): 120 KCl, 10 HEPES, 10 ethylene glycol tetraacetic acid (EGTA), 1.5 Na2ATP, 9.65 CaCl2 (estimated free [Ca^{2+}], 1 μM), 2.34 $MgCl_2$, pH 7.4, adjusted with KOH. To assess the activation efficiency of CAD-1883, a low free [Ca^{2+}] pipette (internal) solution was used, which contained (in mM): 144 KCl, 10 Hepes, 10 EGTA, 1.205 $MgCl_2$, and 7.5 $CaCl_2$ (estimated free [Ca^{2+}], 300 nM), pH 7.3, adjusted with KOH. Free [Ca^{2+}] concentrations were calculated using MaChelator software the software by C. Patton of Stanford University (https://somapp.ucdmc.ucdavis.edu/pharmacology/bers/maxchelator/downloads.htm). Currents were recorded by applying repetitive 1 s voltage ramps from −100 to +100 mV from a holding potential of 0 mV.

For the apamin-related recording experiments, apamin was dissolved in double-distilled water to prepare a stock solution of 100 μM. The stock solution was subsequently diluted with the external solution to achieve the desired working concentrations. An eight-channel (each channel having a volume capacity of 20 mL) gravity perfusion system was used for modulator delivery. After successful cell membrane rupture and establishment of a stable seal, modulators at the desired working concentrations were perfused continuously at a constant flow rate. Simultaneously, a peristaltic pump was employed to steadily remove solution from the recording chamber, enabling full exchange of the external solution throughout the recording. For UCL1684, CAD-1883, and AP30663, these small molecules were dissolved in DMSO to prepare stock solutions with concentrations of 10 mM, 100 mM, and 10 mM, respectively. The perfusion of these three small-molecule modulators was performed similarly to that described above.

Data availability

The cryo-EM density maps of human SK2-apamin, SK2-UCL1684, SK2-CAD-1883, and SK2-AP30663 have been deposited into the Electron Microscopy Data Bank (EMDB) under accession codes EMD-65357 [https://www.emdataresource.org/EMD-65357], EMD-65359 [https://www.emdataresource.org/EMD-65359], EMD-65358 [https://www.emdataresource.org/EMD-65358], and EMD-65356 [https://www.emdataresource.org/EMD-65356], respectively. The coordinates of human SK2-apamin, SK2-UCL1684, SK2-CAD, and SK2-AP have been deposited into the Protein Data Bank (PDB) under accession codes 9VUA [http://doi.org/10.2210/pdb9VUA/pdb], 9VUC [http://doi.org/10.2210/pdb9VUC/pdb], 9VUB [http://doi.org/10.2210/pdb9VUB/pdb], and 9VU9 [http://doi.org/10.2210/pdb9VU9/pdb], respectively. Previously published data for the structures used in this study are available with PDB accession codes: SK4, 6CNO [https://doi.org/10.2210/pdb6CNO/pdb], 6CNM [https://doi.org/10.2210/pdb6CNM/pdb], and 6CNN [https://doi.org/10.2210/pdb6CNN/pdb]; apamin, 7OXF [https://doi.org/10.2210/pdb7OXF/pdb]; Shaker Kv channel, 7SJ1

[https://doi.org/10.2210/pdb7SJ1/pdb]; rat SK2, 8V2H [https://doi.org/10.2210/pdb8V2H/pdb] and 8V3G [https://doi.org/10.2210/pdb8V3G/pdb]; human SK2-4 chimera, 9O52 [https://doi.org/10.2210/pdb9O52/pdb]. The source data underlying Figures 2, 3, 4 and Supplementary Figures 1, 7, 9, and 10 are provided as a Source Data file.

REFERENCES

1 Adelman, J. P., Maylie, J. & Sah, P. Small-conductance Ca2+-activated K+ channels: form and function. *Annu Rev Physiol* **74**, 245-269, doi:10.1146/annurev-physiol-020911-153336 (2012).

2 Bond, C. T. *et al.* Small conductance Ca2+-activated K+ channel knock-out mice reveal the identity of calcium-dependent afterhyperpolarization currents. *J Neurosci* **24**, 5301-5306, doi:10.1523/JNEUROSCI.0182-04.2004 (2004).

3 Stocker, M. Ca(2+)-activated K+ channels: molecular determinants and function of the SK family. *Nat Rev Neurosci* **5**, 758-770, doi:10.1038/nrn1516 (2004).

4 Zhang, W. H. *et al.* Chronic Stress Causes Projection-Specific Adaptation of Amygdala Neurons via Small-Conductance Calcium-Activated Potassium Channel Downregulation. *Biol Psychiatry* **85**, 812-828, doi:10.1016/j.biopsych.2018.12.010 (2019).

5 Wolfart, J., Neuhoff, H., Franz, O. & Roeper, J. Differential expression of the small-conductance, calcium-activated potassium channel SK3 is critical for pacemaker control in dopaminergic midbrain neurons. *J Neurosci* **21**, 3443-3456, doi:10.1523/JNEUROSCI.21-10-03443.2001 (2001).

6 Stackman, R. W. *et al.* Small conductance Ca2+-activated K+ channels modulate synaptic plasticity and memory encoding. *J Neurosci* **22**, 10163-10171, doi:10.1523/JNEUROSCI.22-23-10163.2002 (2002).

7 Hammond, R. S. *et al.* Small-conductance Ca2+-activated K+ channel type 2 (SK2) modulates hippocampal learning, memory, and synaptic plasticity. *J Neurosci* **26**, 1844-1853, doi:10.1523/JNEUROSCI.4106-05.2006 (2006).

8 Kohler, M. *et al.* Small-conductance, calcium-activated potassium channels from mammalian brain. *Science* **273**, 1709-1714, doi:10.1126/science.273.5282.1709 (1996).

9 Stocker, M. & Pedarzani, P. Differential distribution of three Ca(2+)-activated K(+) channel subunits, SK1, SK2, and SK3, in the adult rat central nervous system. *Mol Cell Neurosci* **15**, 476-493, doi:10.1006/mcne.2000.0842 (2000).

10 Ishii, T. M. *et al.* A human intermediate conductance calcium-activated potassium channel. *Proc Natl Acad Sci U S A* **94**, 11651-11656, doi:10.1073/pnas.94.21.11651 (1997).

11 Joiner, W. J., Wang, L. Y., Tang, M. D. & Kaczmarek, L. K. hSK4, a member of a novel subfamily of calcium-activated potassium channels. *Proc Natl Acad Sci U S A* **94**, 11013-11018, doi:10.1073/pnas.94.20.11013 (1997).

12 Sailer, C. A. *et al.* Regional differences in distribution and functional expression of small-conductance Ca2+-activated K+ channels in rat brain. *J Neurosci* **22**, 9698-9707, doi:10.1523/JNEUROSCI.22-22-09698.2002 (2002).

13 Xia, X. M. *et al.* Mechanism of calcium gating in small-conductance calcium-activated potassium channels. *Nature* **395**, 503-507, doi:10.1038/26758 (1998).

14 Fanger, C. M. *et al.* Calmodulin mediates calcium-dependent activation of the intermediate conductance KCa channel, IKCa1. *J Biol Chem* **274**, 5746-5754, doi:10.1074/jbc.274.9.5746 (1999).

15 Lee, C. H. & MacKinnon, R. Activation mechanism of a human SK-calmodulin channel complex elucidated by cryo-EM structures. *Science* **360**, 508-513, doi:10.1126/science.aas9466 (2018).

16 Nam, Y. W. *et al.* Cryo-EM structures of the small-conductance Ca(2+)-activated K(Ca)2.2 channel. *Nat Commun* **16**, 3690, doi:10.1038/s41467-025-59061-1 (2025).

17 Cassell S. J., L. W., Krautwald S., Khoshouei M., Lee Y. T., Hou J., Guan W., Peukert S., Weihofen W. A., Whicher J. R. Mechanism of SK2 channel gating and its modulation by the bee toxin apamin and small molecules. *eLife*, doi:https://doi.org/10.7554/eLife.107733.2 (2025).

18 Hugues, M., Romey, G., Duval, D., Vincent, J. P. & Lazdunski, M. Apamin as a selective blocker of the calcium-dependent potassium channel in neuroblastoma cells: voltage-clamp and biochemical characterization of the toxin receptor. *Proc Natl Acad Sci U S A* **79**, 1308-1312, doi:10.1073/pnas.79.4.1308 (1982).

19 Messier, C. *et al.* Effect of apamin, a toxin that inhibits Ca(2+)-dependent K+ channels, on learning and memory processes. *Brain Res* **551**, 322-326, doi:10.1016/0006-8993(91)90950-z (1991).

20 Burgess, G. M., Claret, M. & Jenkinson, D. H. Effects of quinine and apamin on the calcium-dependent potassium permeability of mammalian hepatocytes and red cells. *J Physiol* **317**, 67-90, doi:10.1113/jphysiol.1981.sp013814 (1981).

21 Grunnet, M., Jensen, B. S., Olesen, S. P. & Klaerke, D. A. Apamin interacts with all subtypes of cloned small-conductance Ca2+-activated K+ channels. *Pflugers Arch* **441**, 544-550, doi:10.1007/s004240000447 (2001).

22 Strobaek, D., Jorgensen, T. D., Christophersen, P., Ahring, P. K. & Olesen, S. P. Pharmacological characterization of small-conductance Ca(2+)-activated K(+) channels stably expressed in HEK 293 cells. *Br J Pharmacol* **129**, 991-999, doi:10.1038/sj.bjp.0703120 (2000).

23 Ishii, T. M., Maylie, J. & Adelman, J. P. Determinants of apamin and d-tubocurarine block in SK potassium channels. *J Biol Chem* **272**, 23195-23200, doi:10.1074/jbc.272.37.23195 (1997).

24 Nolting, A., Ferraro, T., D'Hoedt, D. & Stocker, M. An amino acid outside the pore region influences apamin sensitivity in small conductance Ca2+-activated K+ channels. *J Biol Chem* **282**, 3478-3486, doi:10.1074/jbc.M607213200 (2007).

25 Lamy, C. *et al.* Allosteric block of KCa2 channels by apamin. *J Biol Chem* **285**, 27067-27077, doi:10.1074/jbc.M110.110072 (2010).

26 Weatherall, K. L., Seutin, V., Liégeois, J. F. & Marrion, N. V. Crucial role of a shared extracellular loop in apamin sensitivity and maintenance of pore shape of small-conductance calcium-activated potassium (SK) channels. *Proc Natl Acad Sci U S A* **108**, 18494-18499, doi:10.1073/pnas.1110724108 (2011).

27 Finlayson, K. *et al.* Characterisation of [(125)I]-apamin binding sites in rat brain membranes with HE293 cells transfected with SK channel subtypes. *Neuropharmacology* **41**, 341-350, doi:10.1016/s0028-3908(01)00067-3 (2001).

28 Castle, N. A., Haylett, D. G., Morgan, J. M. & Jenkinson, D. H. Dequalinium: a potent inhibitor of apamin-sensitive K+ channels in hepatocytes and of nicotinic responses in skeletal muscle. *Eur J Pharmacol* **236**, 201-207, doi:10.1016/0014-2999(93)90590-e (1993).

29 Campos Rosa, J. *et al.* Synthesis, molecular modeling, and pharmacological testing of bis-quinolinium cyclophanes: potent, non-peptidic blockers of the apamin-sensitive Ca(2+)-activated K(+) channel. *J Med Chem* **43**, 420-431, doi:10.1021/jm9902537 (2000).

30 Chen, J. Q., Galanakis, D., Ganellin, C. R., Dunn, P. M. & Jenkinson, D. H. bis-Quinolinium cyclophanes: 8,14-diaza-1,7(1, 4)-diquinolinacyclotetradecaphane (UCL 1848), a highly potent and selective, nonpeptidic blocker of the apamin-sensitive Ca(2+)-activated K(+) channel. *J Med Chem* **43**, 3478-3481, doi:10.1021/jm000904v (2000).

31 Wulff, H., Kolski-Andreaco, A., Sankaranarayanan, A., Sabatier, J. M. & Shakkottai, V. Modulators of small- and intermediate-conductance calcium-activated potassium channels and their therapeutic indications. *Curr Med Chem* **14**, 1437-1457, doi:10.2174/092986707780831186 (2007).

32 Brown, B. M., Shim, H., Christophersen, P. & Wulff, H. Pharmacology of Small- and Intermediate-Conductance Calcium-Activated Potassium Channels. *Annu Rev Pharmacol Toxicol* **60**, 219-240, doi:10.1146/annurev-pharmtox-010919-023420 (2020).

33 Bentzen, B. H. *et al.* Mechanisms of Action of the KCa2-Negative Modulator AP30663, a Novel Compound in Development for Treatment of Atrial Fibrillation in Man. *Front Pharmacol* **11**, 610, doi:10.3389/fphar.2020.00610 (2020).

34 Gal, P. *et al.* First Clinical Study with AP30663 - a K(Ca) 2 Channel Inhibitor in Development for Conversion of Atrial Fibrillation. *Clin Transl Sci* **13**, 1336-1344, doi:10.1111/cts.12835 (2020).

35 Holst, A. G. *et al.* Inhibition of the K(Ca)2 potassium channel in atrial fibrillation: a randomized phase 2 trial. *Nat Med* **30**, 106-111, doi:10.1038/s41591-023-02679-9 (2024).

36 Yfanti, C. *et al.* A phase 1 trial of AP30663, a K(Ca)2 channel inhibitor in development for conversion of atrial fibrillation. *Br J Clin Pharmacol* **90**, 1027-1035, doi:10.1111/bcp.15973 (2024).

37 Cho, L. T. *et al.* An Intracellular Allosteric Modulator Binding Pocket in SK2 Ion Channels Is Shared by Multiple Chemotypes. *Structure* **26**, 533-544 e533, doi:10.1016/j.str.2018.02.017 (2018).

38 Zhang, M., Pascal, J. M., Schumann, M., Armen, R. S. & Zhang, J. F. Identification of the functional binding pocket for compounds targeting small-conductance Ca(2)(+)-activated potassium channels. *Nat Commun* **3**, 1021, doi:10.1038/ncomms2017 (2012).

39 Zhang, M., Pascal, J. M. & Zhang, J. F. Unstructured to structured transition of an intrinsically disordered protein peptide in coupling Ca(2)(+)-sensing and SK channel activation. *Proc Natl Acad Sci U S A* **110**, 4828-4833, doi:10.1073/pnas.1220253110 (2013).

40 Wemmer, D. & Kallenbach, N. R. Structure of apamin in solution: a two-dimensional nuclear magnetic resonance study. *Biochemistry* **22**, 1901-1906, doi:10.1021/bi00277a025 (1983).

41 Le-Nguyen, D. *et al.* Role of Asn(2) and Glu(7) residues in the oxidative folding and on the conformation of the N-terminal loop of apamin. *Biopolymers* **86**, 447-462, doi:10.1002/bip.20755 (2007).

42 Kuzmenkov, A. I. *et al.* Apamin structure and pharmacology revisited. *Front Pharmacol* **13**, 977440, doi:10.3389/fphar.2022.977440 (2022).

43 Jumper, J. *et al.* Highly accurate protein structure prediction with AlphaFold. *Nature* **596**, 583-589, doi:10.1038/s41586-021-03819-2 (2021).

44 Labbe-Jullie, C. *et al.* Binding and toxicity of apamin. Characterization of the active site. *Eur J Biochem* **196**, 639-645, doi:10.1111/j.1432-1033.1991.tb15860.x (1991).

45 Bagneris, C. *et al.* Prokaryotic NavMs channel as a structural and functional model for eukaryotic sodium channel antagonism. *Proc Natl Acad Sci U S A* **111**, 8428-8433, doi:10.1073/pnas.1406855111 (2014).

46 Simó-Vicens, R. *et al.* A new negative allosteric modulator, AP14145, for the study of small conductance calcium-activated potassium (K(Ca) 2) channels. *Br J Pharmacol* **174**, 4396-4408, doi:10.1111/bph.14043 (2017).

47 Tan, X. F. *et al.* Structure of the Shaker Kv channel and mechanism of slow C-type inactivation. *Sci Adv* **8**, eabm7814, doi:10.1126/sciadv.abm7814 (2022).

48 Punjani, A., Rubinstein, J. L., Fleet, D. J. & Brubaker, M. A. cryoSPARC: algorithms for rapid unsupervised cryo-EM structure determination. *Nat Methods* **14**, 290-296, doi:10.1038/nmeth.4169 (2017).

49 Pettersen, E. F. *et al.* UCSF Chimera--a visualization system for exploratory research and analysis. *J Comput Chem* **25**, 1605-1612, doi:10.1002/jcc.20084 (2004).

50 Emsley, P. & Cowtan, K. Coot: model-building tools for molecular graphics. *Acta Crystallogr D Biol Crystallogr* **60**, 2126-2132, doi:10.1107/s0907444904019158 (2004).

51 Adams, P. D. *et al.* PHENIX: a comprehensive Python-based system for macromolecular structure solution. *Acta Crystallogr D Biol Crystallogr* **66**, 213-221, doi:10.1107/s0907444909052925 (2010).

52 Pettersen, E. F. *et al.* UCSF ChimeraX: Structure visualization for researchers, educators, and developers. *Protein Sci* **30**, 70-82, doi:10.1002/pro.3943 (2021).

Acknowledgements

We thank Dr. B. Xu at the Cryo-EM Center of the School of Advanced Agricultural Sciences of Peking University and D. Sun at the Cryo-EM Facility at the Institute of Physics, Chinese Academy of Science & Beijing Branch of Songshan Lake Materials Laboratory for support in cryo-EM data collection. We thank Dr. Lu Ma and Wei Fan for their research assistance service. This work is funded by the National Natural Science Foundation of China (32222034 and U25A2080 to W.Z.; 32271272 and T2221001 to D.J.; 82430048 and 82125010 to B.P.), the Natural Science Foundation of Jiangxi Province (20252BAC230007 to W.Z.; 20242BAB24003 to B.P.), and the Taishan Scholars Program (tsqnz20231243 to C.C.). This work is also supported by the Medical-Engineering Interdisciplinary Talent Development Program and Fund of School of Basic Medical Sciences, Jiangxi Medical College, Nanchang University.

Author Contributions

D.J., W.Z., and B.P. conceived and designed the experiments. B.M. prepared samples for the cryo-EM study and made all the constructs. D.W., B.M., Z.X., and C.C. collected the cryo-EM data. D.W. and D.J. processed the data and built and refined the models. E.C. and Z.W. performed the electrophysiology experiments. B.M. and D.W. prepared the figures. B.M., D.W., E.C., C.C., L.S., B.P., W.Z., and D.J. analysed and interpreted the results. D.J. and D.W. wrote the paper, and all the authors reviewed and revised the paper.

Competing Interests

The authors declare no competing interests.

Figure Legends

Figure 1. Cryo-EM structure of human SK2 in complex with CaM.

a, Cryo-EM density map of the human SK2-CaM complex viewed from membrane plane (left), extracellular side (middle), and cytosol (right). Four promoters of SK2 are shown in pink, orange, purple, and cyan, and CaM in yellow. **b,** Cartoon representation of SK2-CaM complex. The same colour scheme from panel a is applied. Calcium ions and lipids are depicted in green spheres and grey sticks, respectively. **c,** The binding of CaM to one protomer of SK2. CaM interacting with the S4-S5 linker and the HA helix are coloured in grey and yellow, respectively. **d,** Superposition of SK2 (pink) and SK4 (grey, PDB ID: 6cnn). Detailed interactions between S3 and S4 helices are shown in right. A cholesterol-like density in SK2 is shown in green meshes. DDM in SK4 is depicted in wheat sticks.

Figure 2. Structural basis for SK2 blockade by apamin and UCL1684.

a, Sequence of apamin and chemical structure of UCL-1684. Arg13 and Arg14 of apamin are show as red. **b,** Concentration-dependent inhibition of SK2 by apamin. Left, representative current traces of SK2-expressing HEK293 cells. Data are normalized and presented as mean values ± SEM (n=8 cells). **c,** Cryo-EM density map of SK2-apamin. SK2 in grey, apamin in red. **d,** Apamin binds to the outer vestibule of SK2. Residues involved in apamin binding are shown as sticks. Apamin in red, SK2 in green, purple, orange, and pink, respectively. K^+ ions are depicted in blue spheres. **e,** Interactions between apamin and the S3-S4 loop. Black dashed lines indicate polar interactions. **f,** UCL-1684 binds in the outer vestibule of SK2. UCL-1684 is shown as yellow sticks. **g,** Inhibition of SK2 variants by apamin and UCL-1684. Data are shown as mean ± SEM (n = 6 cells) of normalized currents recorded from HEK293 cells expressing A242F, F243A, S244F, Y245A, H336N, and N367H in response to 300 nM apamin or 1 μM UCL1684. **h,** Concentration-dependent inhibition curves of SK2 variants by apamin. Data were normalized and presented as mean values ± SEM (WT, n=8; R240A, n=8; S244F, n=9; Y245A, n=8; N367H, n=8 cells). Source Data are provided as a Source Data file.

Figure 3. Structural basis for SK2 potentiation by CAD-1883.

a, Chemical structure of CAD-1883. **b,** Concentration-dependent activation curve of SK2 by CAD-1883. Representative whole-cell current traces of SK2 enhanced by CAD-1883. Voltage ramp, -100 mV to 100 mV (Left). Data are presented as mean values ± SEM (n = 8 cells). Curve was fitted using nonlinear regression. **c,** Cryo-EM density map of CAD-1883 in SK2-CAD-1883 complex. Density maps for CAD-1883 and interacting residues are shown in purple and grey meshes, respectively. **d,** Detailed interactions between CAD-1883 and SK2-CaM complex. CAD-1883 in cyan sticks, residues involved in CAD-1883 binding are shown in sticks. **e**-**h,** CAD-1883 stimulated current traces of WT SK2 (**e**), L291W (**f**), L291F (**g**), and LN291-292AA (**h**). The free Ca^{2+} concentration in internal solution is 300 nM. CAD-1883 is applied to the external solution at 100 μM. **i,** Pore radius analysis of SK2-apamin and SK2-CAD-1883 by HOLE. Two opposing subunits are shown as cartoon; pores of SK2-apamin and SK2-CAD-1883 are shown as pink and yellow, respectively. **j,** Pore radius profiles of SK2-apamin and SK2-CAD-1883 along the pore axis. Selectivity filter (SF) and activation gate (AG) regions are shaded in pink and light blue. **k,** Superposition of SK2-CAD-1883 (cyan) and opened SK4 (grey, PDB: 6cno). Black arrows indicate conformational changes. Source Data are provided as a Source Data file.

Figure 4. Structural basis for SK2 inhibition by AP30663.

a, Chemical structure of AP30663. **b,** Concentration-dependent inhibition curve of SK2 by AP30663. Left, representative whole-cell current traces of SK2 inhibited by AP30663. Voltage ramp, -100 mV to 100 mV (Left). Data are presented as mean values ± SEM (n = 8 cells). Curve was fitted using nonlinear regression. **c,** Cryo-EM structure of SK2-AP30663. SK2-AP30663 in pink sticks. **d,** Cryo-EM density map of AP30663 in the central cavity of SK2-AP30663 (left). As a comparison, no such density is observed in SK2-apamin. Density maps for AP30663 and SK2 are shown in pink and grey, respectively. K^+ ions depicted as blue spheres. **e,** Interactions between AP30663 and SK2 complex. Residues are indicated with black lines. **f,** Inhibitory effects of 30 μM AP30663 on SK2 variants. Data are normalized and presented as mean values ± SEM (WT, n=6; A383F, n=5; A383L, n=6; T386L, n=7; T386F, n=5 cells). **g,** Representative whole-cell current trace of mutation A383L inhibited by AP30663, elicited by voltage ramps (−100 mV to +100 mV). **h,** Concentration-dependent inhibition curve of SK2-A383L by AP30663. Data are presented as mean values ± SEM (n = 7 cells). Curve was fitted using nonlinear regression. The free Ca^{2+} in the internal solution for all AP30663 related test is 1 μM. Source Data are provided as a Source Data file.

Figure 5. Proposed model of SK2 activation and modulation.

a, When intracellular Ca^{2+} at low levels, SK2 channel assumes a closed resting state. The C-lobe of CaM binds to the HA helix of SK2, while the N-lobe is dynamic. **b**, After intracellular Ca^{2+} increased to sub-micromolar levels, Ca^{2+} ions bind to CaM N-lobe and induce conformational changes that facilitate the engagement of CaM N-lobe and the $S_{45}A$ helix, resulting in pore opening. **c**, Multiple modulations sites in SK2-CaM complex. Site 1 in the outer vestibule for apamin and UCL1684; Site 2 in the central cavity for AP30663 analogues; Site3 in the CaM N-lobe and SK2 $S_{45}A$ helix interface for activators such as CAD-1883 and NS-309.

Editorial Summary:

SK2 channel regulates the intrinsic excitability and firing frequency of excitable cells. Here, authors present the cryo-EM structures of human SK2 with apamin and three modulators, revealing the structural basis for activation and inhibition of SK2.

Peer review information: *Nature Communications* thanks Wei Lü who co-reviewed with Sushant Kumar; Heike Wulff and the other, anonymous, reviewer(s) for their contribution to the peer review of this work. A peer review file is available.

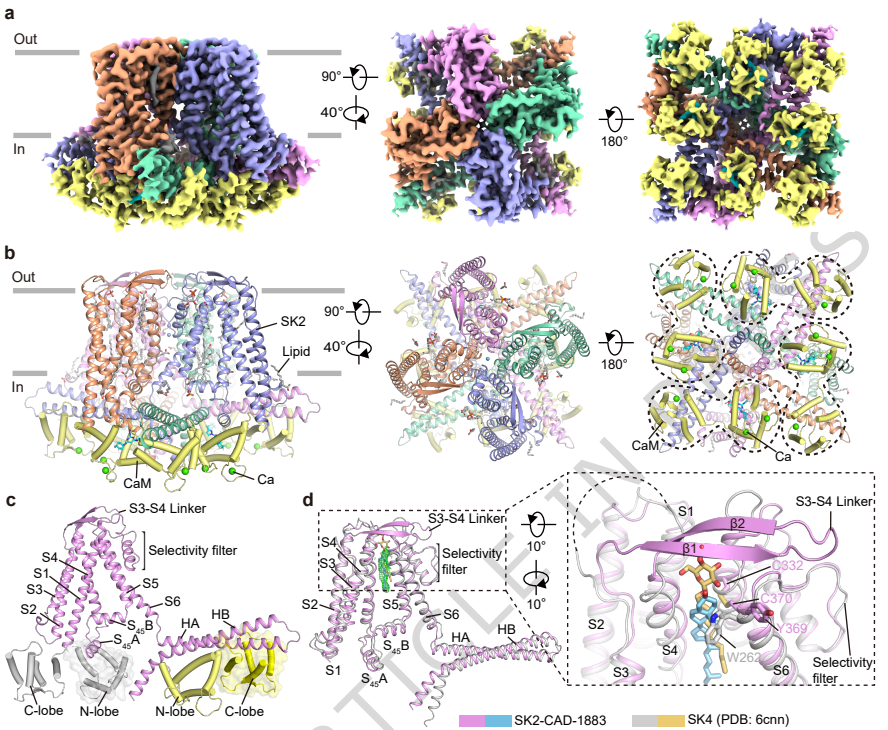

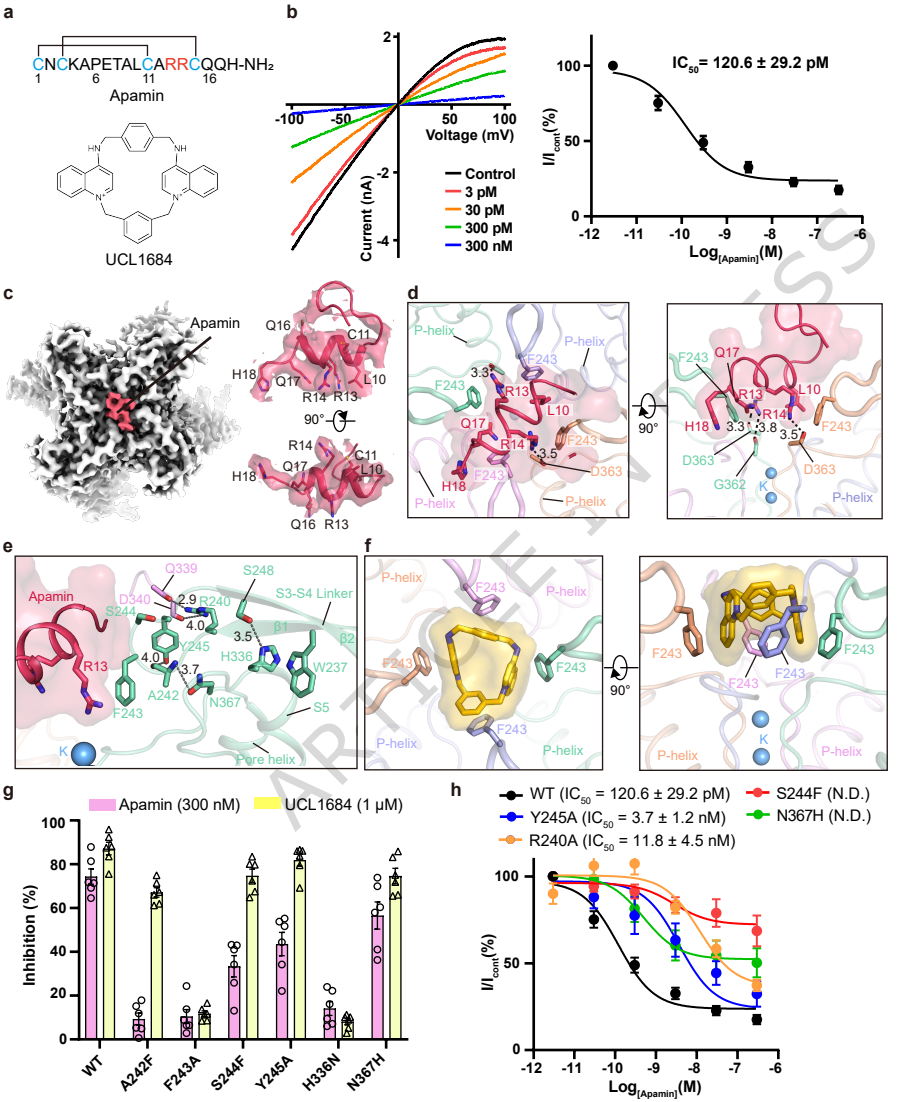
a
CNCKAPETALCARRCQQH-NH2
1 6 11 16
Apamin
UCL1684
b
Current (nA)
Voltage (mV)
Control
3 pM
30 pM
300 pM
300 nM
IC50= 120.6 ± 29.2 pM
I/Icont (%)
Log[Apamin](M)
c
Apamin
Q16
C11
H18
Q17
L10
R14
R13
90°
d
P-helix
F243
R13
L10
Q17
R14
H18
D363
90°
e
Apamin
Q339
S248
D340
S244
R240
S3-S4 Linker
Y245
H336
β1
β2
W237
A242
N367
S5
R13
F243
K
Pore helix
f
P-helix
F243
90°
g
Apamin (300 nM)
UCL1684 (1 μM)
Inhibition (%)
WT
A242F
F243A
S244F
Y245A
H336N
N367H
h
WT (IC50 = 120.6 ± 29.2 pM)
Y245A (IC50 = 3.7 ± 1.2 nM)
R240A (IC50 = 11.8 ± 4.5 nM)
S244F (N.D.)
N367H (N.D.)
I/Icont (%)
Log[Apamin](M)